

Anderson localization on the Cayley tree : multifractal statistics of the transmission at criticality and off criticality

Cécile Monthus and Thomas Garel

Institut de Physique Théorique, CNRS and CEA Saclay 91191 Gif-sur-Yvette cedex, France

In contrast to finite dimensions where disordered systems display multifractal statistics only at criticality, the tree geometry induces multifractal statistics for disordered systems also off criticality. For the Anderson tight-binding localization model defined on a tree of branching ratio $K = 2$ with N generations, we consider the Miller-Derrida scattering geometry [J. Stat. Phys. 75, 357 (1994)], where an incoming wire is attached to the root of the tree, and where K^N outgoing wires are attached to the leaves of the tree. In terms of the K^N transmission amplitudes t_j , the total Landauer transmission is $T \equiv \sum_j |t_j|^2$, so that each channel j is characterized by the weight $w_j = |t_j|^2/T$. We numerically measure the typical multifractal singularity spectrum $f(\alpha)$ of these weights as a function of the disorder strength W and we obtain the following conclusions for its left-termination point $\alpha_+(W)$. In the delocalized phase $W < W_c$, $\alpha_+(W)$ is strictly positive $\alpha_+(W) > 0$ and is associated with a moment index $q_+(W) > 1$. At criticality, it vanishes $\alpha_+(W_c) = 0$ and is associated with the moment index $q_+(W_c) = 1$. In the localized phase $W > W_c$, $\alpha_+(W) = 0$ is associated with some moment index $q_+(W) < 1$. We discuss the similarities with the exact results concerning the multifractal properties of the Directed Polymer on the Cayley tree.

I. INTRODUCTION

Since its discovery fifty years ago [1] Anderson localization has remained a very active field of research (see for instance the reviews [2–7]). According to the scaling theory [8], there is no delocalized phase in dimensions $d = 1, 2$, whereas there exists a localization/delocalization at finite disorder in dimension $d > 2$. To get some insight into this type of transition, it is natural to consider Anderson localization on the Cayley tree which is expected to represent some mean-field limit. The tight-binding Anderson model on the Cayley tree has been thus studied by various techniques over the years [9–14]. Other studies have focused on random-scattering models on the Cayley tree [15–17]. For the version of the model defined on random regular graph of fixed degree, we refer to the recent work [18] and references therein. The motivation to study Anderson localization on the Cayley tree has been revived recently by the question of many-body localization [19], because the geometry of the Fock space of many-body states was argued to be similar to a Cayley tree [20–26]. But of course, the questions on many-body localization are much more difficult and are still debated in the recent studies [22, 25–31].

In quantum coherent problems, the most appropriate characterisation of transport properties consists in defining a scattering problem where the disordered sample is linked to incoming wires and outgoing wires and in studying the reflection and transmission coefficients. This scattering theory definition of transport, first introduced by Landauer [32], has been much used for one-dimensional systems [33–35] and has been generalized to higher dimensionalities and multi-probe measurements (see the review [36] and references therein). For the Anderson model on the Cayley tree, an appropriate scattering geometry has been introduced by Miller and Derrida [13] to perform weak-disorder expansions and numerical computations : an incoming wire is attached to the root, and K^N outgoing wires are attached to the leaves of a tree of branching ratio K with N generations. In a previous work [14], we have used this scattering geometry to study numerically the statistical properties of total the Landauer transmission $T \equiv \sum_j |t_j|^2$ as a function of the number N of generations and of the disorder strength and to measure its critical behavior. The aim of this paper is to characterize the spatial inhomogeneity between the various channels j : the weights $|t_j|^2/T$ of the K^N channels turn out to present a multifractal statistics, not only at criticality but also in the localized and delocalized phases as a consequence of the tree geometry. So we analyse how the singularity spectrum $f(\alpha)$ changes as a function of the disorder strength.

The paper is organized as follows. In section II, we introduce the Anderson localization tight-binding model on the Cayley tree and the scattering geometry that we consider to study the multifractal statistics of the Landauer transmission. Our numerical results concerning the multifractal statistics in various phases are described in sections III and IV for the Box distribution and for the Cauchy distribution of disorder respectively. Our conclusions are summarized in section V. In Appendix A, we recall the exactly known results concerning the multifractality for the Directed Polymer on the Cayley tree, as a classical model which is useful to consider as a comparison, both for conceptual and numerical purposes. Appendix B explains how the numerical singularity spectra presented on figures have been obtained.

II. SCATTERING GEOMETRY FOR ANDERSON LOCALIZATION ON THE CAYLEY TREE

A. Anderson tight-binding model on the Cayley tree

We consider the Anderson tight-binding model

$$H = \sum_i \epsilon_i |i\rangle\langle i| + \sum_{\langle i,j \rangle} |i\rangle\langle j| \quad (1)$$

where the hopping between nearest neighbors $\langle i, j \rangle$ is a constant $V = 1$ and where the on-site energies ϵ_i are independent random variables drawn from the 'Box' distribution

$$p_{Box}(\epsilon) = \frac{1}{W} \theta\left(-\frac{W}{2} \leq \epsilon \leq \frac{W}{2}\right) \quad (2)$$

The parameter W thus represents the disorder strength. We have also studied the case of the Cauchy disorder

$$p_{Cauchy}(\epsilon) = \frac{W}{\pi(\epsilon^2 + W^2)} \quad (3)$$

B. Miller-Derrida scattering geometry

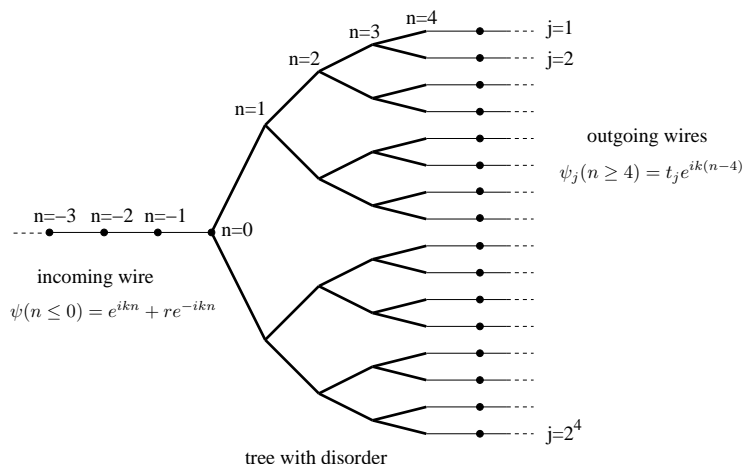


FIG. 1: Scattering geometry of Ref. [13] : the disordered tree of branching ratio $K = 2$ starting at generation $n = 0$ and ending at generation N (on the Figure $N = 4$) is attached to one incoming wire and to K^N outgoing wires. The total transmission is $T \equiv \sum_j |t_j|^2 = 1 - |r|^2$ where r is the reflection amplitude of the incoming wire, and t_j the transmission amplitudes of the outgoing wires.

We consider the scattering geometry introduced in [13] and shown on Fig. 1 : the finite tree of branching ratio K is attached to one incoming wire at its root (generation $n = 0$) and to K^N outgoing wires at generation N . One is interested into the eigenstate $|\psi\rangle$ that satisfies the Schrödinger equation

$$H|\psi\rangle = E|\psi\rangle \quad (4)$$

inside the disorder sample and in the wires where one requires the plane-wave forms

$$\begin{aligned} \psi(n \leq 0) &= e^{ikn} + r e^{-ikn} \\ \psi_j(n \geq N) &= t_j e^{ik(n-N)} \end{aligned} \quad (5)$$

These boundary conditions define the reflection amplitude r of the incoming wire and the transmission amplitudes t_j of the $j = 1, 2, \dots, K^N$ outgoing wires. To satisfy the Schrödinger Equation of Eq. 4 within the wires with the forms of Eq. 5, one has the following relation between the energy E and the wave vector k

$$E = 2 \cos k \quad (6)$$

To simplify the discussion, we will focus in this paper on the case of zero-energy $E = 0$ and wave-vector $k = \pi/2$, because the zero-energy $E = 0$ corresponds to the center of the band where the delocalization first appears when the strength W of the disorder is decreased from the strong disorder localized phase. From the conservation of energy, the total transmission T is related to the reflection coefficient $|r|^2$

$$T \equiv \sum_j |t_j|^2 = 1 - |r|^2 \quad (7)$$

We refer to [13] for the results of a weak disorder expansion within this framework, and for a numerical Monte-Carlo approach to determine the mobility edge in the plane (E, W) . In [14] we have studied the statistical properties over the disordered samples of the total Landauer transmission T_N at zero energy $E = 0$ as a function of the disorder strength W and of the number N of generations. In the localized phase $W > W_c$, the typical transmission $T_N^{typ} \equiv e^{\overline{\ln T_N}}$ decays exponentially with the number N of generations

$$\ln(T_N^{typ}) \equiv \overline{\ln T_N(W > W_c)} \underset{N \rightarrow \infty}{\simeq} -\frac{N}{\xi_{loc}(W)} \quad (8)$$

where ξ_{loc} represents the localization length. In the delocalized phase, the typical transmission remains finite in the limit where the number of generations N diverges

$$T_N^{typ} \equiv e^{\overline{\ln T_N(W < W_c, N)}} \underset{N \rightarrow \infty}{\simeq} T_\infty(W < W_c) > 0 \quad (9)$$

The total Landauer transmission T is thus an appropriate order parameter of the localization transition at the mobility edge W_c . We refer to [14] for more details on the critical behaviors of the localization length ξ_{loc} and of the asymptotic value $T_\infty(W < W_c)$. In the present paper, we wish to analyse the statistics of the contributions t_j of the various channels to the total transmission of Eq. 7 as we now explain.

C. Statistical properties of the weights of the outgoing channels

In each disordered sample, we consider the K^N weights

$$w_j \equiv \frac{|t_j|^2}{T} = \frac{|t_j|^2}{\sum_{j'} |t_{j'}|^2} \quad (10)$$

and the 'analogs' of Inverse Participation Ratios

$$I_q(M = K^N) \equiv \sum_{j=1}^M w_j^q = \frac{\sum_{j=1}^M |t_j|^{2q}}{\left(\sum_{j=1}^M |t_j|^2\right)^q} \quad (11)$$

It is useful to introduce the multifractal formalism with respect to $M = K^N$ (or equivalently the large deviation formalism with respect to the variable $N = (\ln M)/(\ln K)$): one defines the typical exponents $\tau^{typ}(q)$ as the exponents governing the decays of the typical values

$$I_q^{typ}(M = K^N) \equiv e^{\overline{\ln I_q(M)}} \underset{M \rightarrow +\infty}{\propto} M^{-\tau^{typ}(q)} = e^{-N(\ln K)\tau^{typ}(q)} \quad (12)$$

The typical singularity spectrum $f^{typ}(\alpha)$ is defined as follows: in a large disordered sample, the number $\mathcal{N}_M(\alpha)$ of channels j (among the total of M of channels) that have a weight w_j scaling as $w_j \sim M^{-\alpha}$ scales as

$$\mathcal{N}_M^{typ}(\alpha) \simeq M^{f^{typ}(\alpha)} \quad (13)$$

Then saddle-point computation of I_q (Eqs 11 and 12)

$$I_q^{typ}(M = K^N) = \sum_{j=1}^M w_j^q \sim \int d\alpha M^{f^{typ}(\alpha) - q\alpha} \quad (14)$$

leads to the Legendre transform formula

$$-\tau^{typ}(q) = \max_\alpha [f^{typ}(\alpha) - q\alpha] \quad (15)$$

Let us now briefly recall some basic notions about multifractality that will be useful to analyse the numerical results. As a consequence of the weight definition of Eq. 10, the index α cannot be negative, so one has $\alpha \geq 0$. As a consequence of Eq. 13, the 'typical' singularity spectrum is non-negative : $f^{typ}(\alpha) \geq 0$. [Note that this is in contrast with the 'averaged' singularity spectrum $f^{av}(\alpha)$ which can become negative to describe rare events (see [7] for more details), but in this paper we only consider the typical singularity spectrum]. The termination points α_{\pm} are defined as the points where the singularity spectrum vanishes $f(\alpha_{\pm}) = 0$, whereas the singularity spectrum remains strictly positive in between

$$f^{typ}(\alpha) > 0 \text{ for } \alpha_+ < \alpha < \alpha_- \quad (16)$$

The left termination point α_+ which represents the smallest possible α will play an essential role in the following. From the point of view of the Legendre transform formula of Eq. 15, it is associated with some positive value $q_+ > 0$, where the saddle point $\alpha(q)$ reaches α_+ , so that for all higher q , the saddle point remains frozen at this value

$$\alpha(q > q_+) = \alpha_+ \quad (17)$$

and the typical exponent $\tau^{typ}(q)$ is simply

$$\tau^{typ}(q > q_+) = q\alpha_+ \quad (18)$$

The same discussion can be transposed to the right termination point α_- associated with some negative index $q_- < 0$, with $\alpha(q < q_-) = \alpha_-$ and $\tau^{typ}(q < q_-) = q\alpha_-$. The value $q = 0$ is associated with the most probable value $\alpha_0 \equiv \alpha(q = 0)$ where the singularity spectrum reaches its maximum

$$f(\alpha_0) = 1 \quad (19)$$

Finally the value $q = 1$ is associated with the value $\alpha_1 \equiv \alpha(q = 1)$ where the singularity spectrum satisfies

$$f(\alpha_1) = \alpha_1 \quad (20)$$

as a consequence of the normalization $I_{q=1}^{typ} = 1$ corresponding to $\tau^{typ}(q = 1) = 0$.

D. Comparison with Anderson localization models in finite dimension

We should stress here the similarities and differences with the usual multifractal definitions used for Anderson localization models in finite dimension d (see the review [7]) : for a normalized eigenfunction on the volume $V = L^d$ (i.e. $\sum_{r \in V=L^d} |\psi(r)|^2 = 1$), the Inverse Participation ratios are defined as

$$P_q \equiv \sum_{r \in V=L^d} |\psi(r)|^{2q} \quad (21)$$

and the exponents $\tau(q)$ are defined as

$$P_q \underset{L \rightarrow +\infty}{\propto} L^{-\tau^{typ}(q)} \quad (22)$$

In finite dimension d , powers of L and powers of the volume $V = L^d$ correspond to the same scaling (up to a redefinition of the exponents), while on the tree, one should use powers of the number $M = K^N$ in the definitions of Eq. 12, and not powers of the linear distance N .

Another difficulty with the tree geometry is that sites of different generations are not equivalent in the pure case (see [14] for explicit expressions of wavefunctions that decay exponentially with the distance N in the pure case). This shows that direct generalizations of P_q where the sum is over all sites of the tree is not appropriate (see again [14] for more detailed discussion on the anomalous behavior of usual I.P.R.s), and this is why we have chosen to consider the weights of the channels in the Miller-Derrida geometry, since they involve the wave-function weights of the K^N points that are at the same distance N of the origin. In the pure case, these weights have all the same weights $|t_j|^2/T = 1/K^N$ (see again [14] for more details), leading to the mono-fractal behavior of the I_q of Eq. 11

$$I_q^{pure}(M = K^N) = \frac{\sum_{j=1}^{K^N} |t_j|^{2q}}{\left(\sum_{j=1}^{K^N} |t_j|^2\right)^q} = \frac{1}{K^{N(q-1)}} \quad (23)$$

So the tree geometry has the peculiarity to induce multifractal behavior of the I_q even in the delocalized phase (the radial symmetry of the pure case is not able to survive even at small disorder), whereas in any finite dimension, the I.P.R. in the delocalized phase are monofractal with the same scaling as the pure case.

Finally in finite dimension, the localized phase is characterized by localized eigenfunctions where some rare sites have finite weights, whereas most sites have exponentially-small weights in the linear size L . On the tree, all eigenfunctions have to decay exponentially with the distance N , even in the pure case, to fulfill the normalization constraint with an exponentially-growing number of sites with the distance N . So in the localized phase, the fluctuations of the weights will be also characterized by a multifractal statistics of the I_q of Eq. 11.

In summary, in contrast to finite dimensions where disordered systems display multifractal statistics only at criticality, the tree geometry induces multifractal statistics for disordered systems also outside criticality, if one consider the inhomogeneities among the points at a given distance from the center. In the recent mathematical study [37], similar observables have been introduced with a large deviation analysis in N .

Since these multifractal properties of disordered models defined on trees are unusual with respect to finite dimensions, it is useful to see how the multifractal analysis of Eq. 12 works in an exactly solved model : in the Appendix A we thus recall the case of the Directed Polymer on the Cayley tree, which is a classical disordered model having the same geometry.

III. NUMERICAL RESULTS FOR THE BOX DISTRIBUTION

In this section, we describe our numerical results for a tree of branching ratio $K = 2$ where the disordered on-site energies are drawn with the Box distribution of Eq. 2. The critical disorder width W_c at the center of the band $E = 0$ has been found to be numerically in the interval [9, 14, 18]

$$16 < W_c < 18 \quad (24)$$

A. Numerical details

We have studied trees containing N generations with a corresponding number $n_s(N)$ of disordered samples with the values

$$\begin{aligned} N &= 10; 12; 14; 16; 18; 20; 22; 24 \\ n_s(N) &= 10^7; 27.10^5; 7.10^5; 17.10^4; 43.10^3; 10^4; 27.10^2; 650 \end{aligned} \quad (25)$$

We have chosen to work only with even N , because in the pure case, the total Landauer transmission is perfect $T_N^{pure} = 1$ only for even N (see section 2.2 of Ref [14] for more details). The transition amplitudes t_j of the scattering eigenvalue problem of Eqs 4 and 5 are computed via the introduction of Riccati variables as explained in details in [13, 14]. The multifractal spectrum is then obtained via the standard method of Ref [44], where the curve $f(\alpha)$ is obtained parametrically in the parameter q (see Appendix B B for more details) : here we have used values in the range $-5 \leq q \leq +5$. As shown in Appendix A, we have checked that the sizes and statistics of Eq. 25 were sufficient to obtain reliable results for the multifractal properties of the Directed Polymer model by a direct comparison with exactly known results in various phases.

Let us make some final remark to explain the differences with respect to the numerical method used in our previous work concerning the full transmission T . In [14] we had used the so called 'pool method' (see section 2.3.1 of [14]) which allows to study much bigger sizes (like $N \sim 10^5$ generations). This was possible because the full transmission T can be directly computed from the reflection coefficient of the incoming wire alone (see Eq. (17) of [14]), i.e. one does not need to compute the whole set of transmissions t_j of individual channels. So the full transmission T can be obtained directly from the stable probability distribution of the complex Riccati variables, for which the pool method is well adapted. However the multifractal spectrum is a much more complicated observable : it does not depend only on the one-point distribution of the Riccati variables, but it involves the whole correlations between the Riccati variables along branches (each Riccati variable is computed from its K descendants, see Eq. (25) of [14]). Of course one could try to develop some generalized pool method to compute multifractal properties, but one should be very careful to avoid artifacts. In the present paper, we have thus chosen to work only with exact numerical data on finite trees to avoid any doubts on the numerical results.

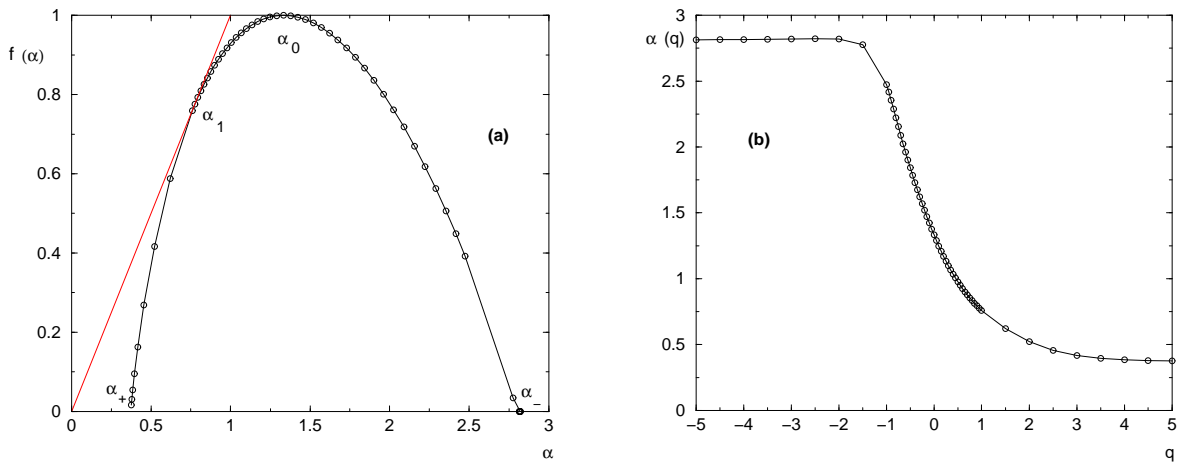


FIG. 2: Box disorder $W = 5$ (a) The singularity spectrum $f(\alpha)$ has for termination points $\alpha_+ \simeq 0.37$ and $\alpha_- \simeq 2.82$, for typical value $\alpha_0 \simeq 1.33$ and for tangent point $\alpha_1 = f(\alpha_1) \simeq 0.76$ (b) The corresponding $\alpha(q)$ saturates at a value around $q_+ \simeq 3$.

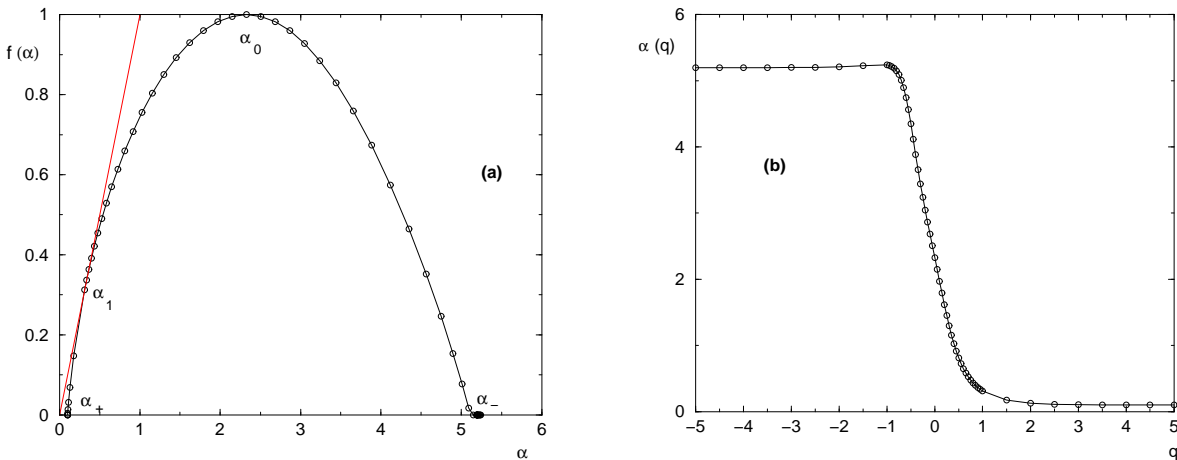


FIG. 3: Box disorder $W = 10$ (a) The singularity spectrum $f(\alpha)$ has for termination points $\alpha_+ \simeq 0.1$ and $\alpha_- \simeq 5.2$, for typical value $\alpha_0 \simeq 2.33$ and for tangent point $\alpha_1 = f(\alpha_1) \simeq 0.31$ (b) The corresponding $\alpha(q)$ saturates at a value around $q_+ \simeq 2$.

B. Delocalized phase

In the delocalized phase $W < W_c$, we find that the left termination point is strictly positive $\alpha_+(W) > 0$ and is associated with a moment index $q_+(W) > 1$. Two examples of our numerical data are shown on Fig. 2 and 3 corresponding to $W = 5$ and $W = 10$ respectively.

C. Critical point

At criticality, the left termination point vanishes $\alpha_+(W_c) = 0$ together with the tangent point $\alpha_1 = f(\alpha_1) = 0$, as shown on Fig. 4 corresponding to $W = 17$. The corresponding saddle-point $\alpha(q)$ saturates at the value $q_+(W_c) \simeq 1$.

D. Localized phase

In the localized phase $W > W_c$, the vanishing left termination point $\alpha_+(W_c) = 0$ is associated with some moment index $q_+(W) < 1$, as shown on Fig. 5 and 6 corresponding to $W = 30$ and $W = 40$ respectively.

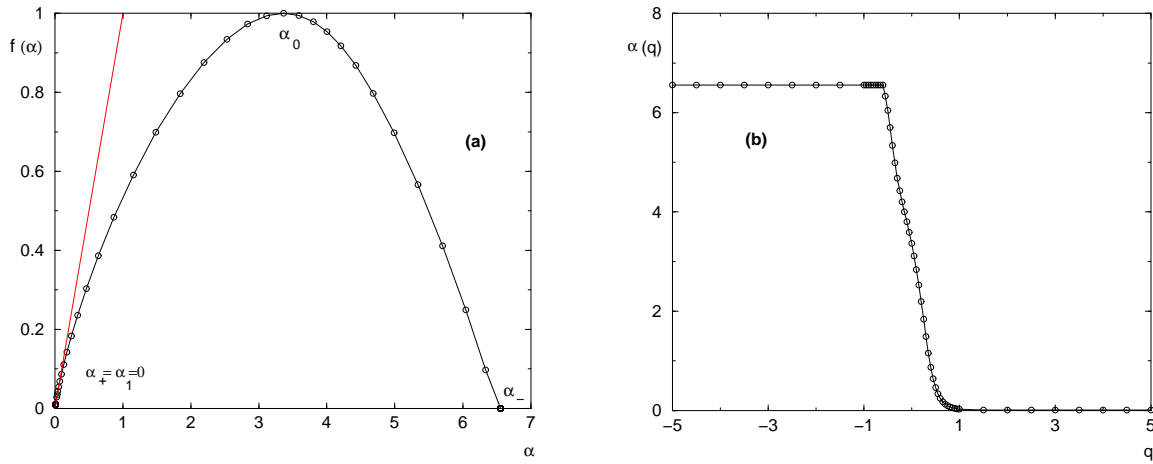


FIG. 4: Box disorder $W = 17$ (a) The singularity spectrum $f(\alpha)$ has for termination points $\alpha_+ \simeq 0$ and $\alpha_- \simeq 6.7$, for typical value $\alpha_0 \simeq 3.36$ and for tangent point $\alpha_1 = f(\alpha_1) \simeq 0$ (b) The corresponding $\alpha(q)$ saturates at the value $q_+ \simeq 1$.

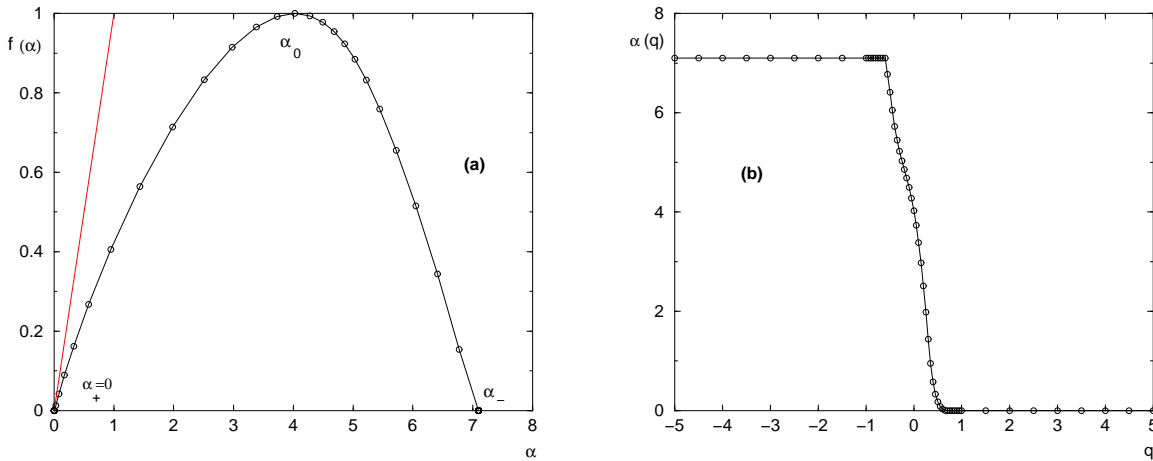


FIG. 5: Box disorder $W = 30$ (a) The singularity spectrum $f(\alpha)$ has for termination points $\alpha_+ = 0$ and $\alpha_- \simeq 7.1$, and for typical value $\alpha_0 \simeq 4.0$ (b) The corresponding $\alpha(q)$ saturates at the value $q_+ \simeq 0.55$.

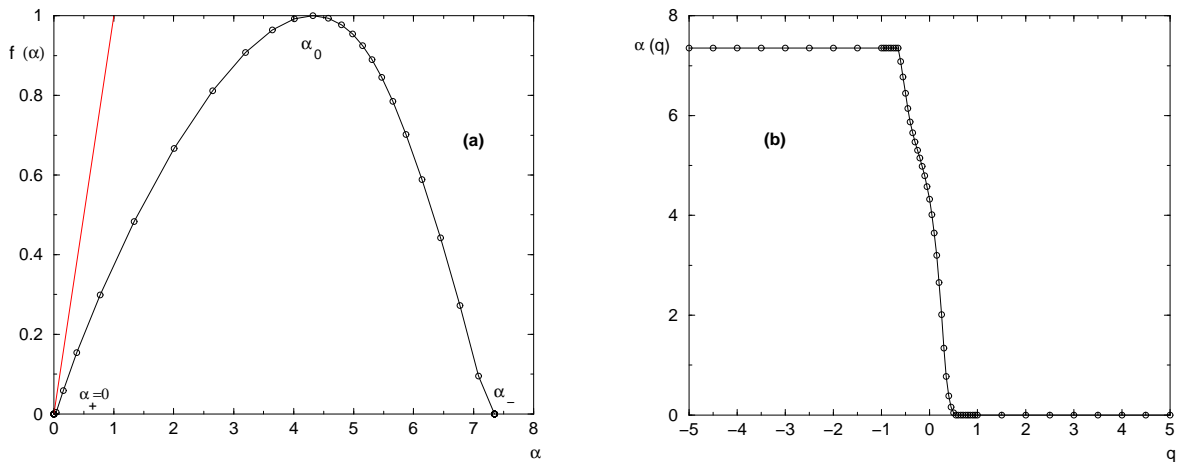


FIG. 6: Box disorder $W = 40$ (a) The singularity spectrum $f(\alpha)$ has for termination points $\alpha_+ \simeq 0$ and $\alpha_- \simeq 7.35$, and for typical value $\alpha_0 \simeq 4.3$. (b) The corresponding $\alpha(q)$ saturates at the value $q_+ \simeq 0.45$.

IV. NUMERICAL RESULTS FOR THE CAUCHY DISTRIBUTION

In this section, we describe our numerical results for a tree of branching ratio $K = 2$ where the disordered on-site energies are drawn with the Cauchy distribution of Eq. 3. The numerical details are the same as in the section III A. The critical disorder width W_c at the center of the band $E = 0$ has been previously found to be numerically in the interval [9]

$$3.6 < W_c < 4.4 \quad (26)$$

In many areas, the Cauchy distribution whose variance is infinite leads to anomalous results with respect to bounded distributions. In the context of Anderson localization, the Cauchy disorder is of course anomalous from the point of view of weak-disorder expansion which contains explicitly the variance of the disorder (see [35] and references therein). However from the point of view of Anderson localization transitions at finite disorder, we are not aware of any statement concerning its anomalous behaviors (except old conclusions concerning the absence of transition that have been shown to be false afterwards). On the theoretical side, the Cauchy distribution is well known to have many advantages : it is the only disorder distribution that leads to an exact and simple solution in one dimension (see [35] and references therein), and that leads to an exact and simple solution for the density of states in any dimension [53]. For the Anderson localization on the Cayley tree that we consider in the present paper, it is also the only disorder distribution that leads to an exact and simple solution for the stationary distribution of the Riccati variables in the localized phase [9, 13], the only remaining problem being that it is not known in the delocalized phase where the Riccati variables are complex [13]. These theoretical advantages of the Cauchy distribution justify to study numerically its properties and to compare with the case of bounded distributions. In the following, we obtain that the results concerning the multifractal properties of the transmission for the Cauchy distribution are qualitatively the same as the results obtained in the previous section concerning the box distribution.

A. Delocalized phase

In the delocalized phase $W < W_c$, we find that the left termination point is strictly positive $\alpha_+(W) > 0$ and is associated with a moment index $q_+(W) > 1$. Two examples of our numerical data are shown on Fig. 7 and 8 corresponding to $W = 0.5$ and $W = 1$ respectively.

B. Critical point

At criticality, the left termination point vanishes $\alpha_+(W_c) = 0$ together with the tangent point $\alpha_1 = f(\alpha_1) = 0$, as shown on Fig. 9 corresponding to $W = 4$. The corresponding saddle-point $\alpha(q)$ saturates at the value $q_+(W_c) \simeq 1$.

C. Localized phase

In the localized phase $W > W_c$, the vanishing left termination point $\alpha_+(W_c) = 0$ is associated with some moment index $q_+(W) < 1$, as shown on Fig. 10 and 11 corresponding to $W = 6$ and $W = 10$ respectively.

V. CONCLUSIONS

In this paper, we have studied the multifractal properties of the Landauer transmission for the Anderson localization tight-binding model on the Cayley tree within the Miller-Derrida scattering geometry. We have explained why, in contrast to finite dimensions where disordered systems display multifractal statistics only at criticality, the tree geometry induces multifractal statistics for disordered systems also off criticality. As an example, we have recalled in the Appendix the exact results concerning the Directed Polymer on the Cayley tree. We have presented numerical results for the typical multifractal singularity spectrum $f(\alpha)$ of the channels weights as a function of the disorder strength W , both the the Box distribution and the Cauchy distribution of disorder. Our main conclusion concerns the left-termination point $\alpha_+(W)$. In the delocalized phase $W < W_c$, $\alpha_+(W)$ is strictly positive $\alpha_+(W) > 0$ and is associated with a moment index $q_+(W) > 1$. At criticality, it vanishes $\alpha_+(W_c) = 0$ and is associated with the moment index $q_+(W_c) = 1$. In the localized phase $W > W_c$, $\alpha_+(W) = 0$ is associated with some moment index $q_+(W) < 1$. These properties of the delocalized and localized phases are thus qualitatively similar to the exact results concerning the Directed Polymer on the Cayley tree.

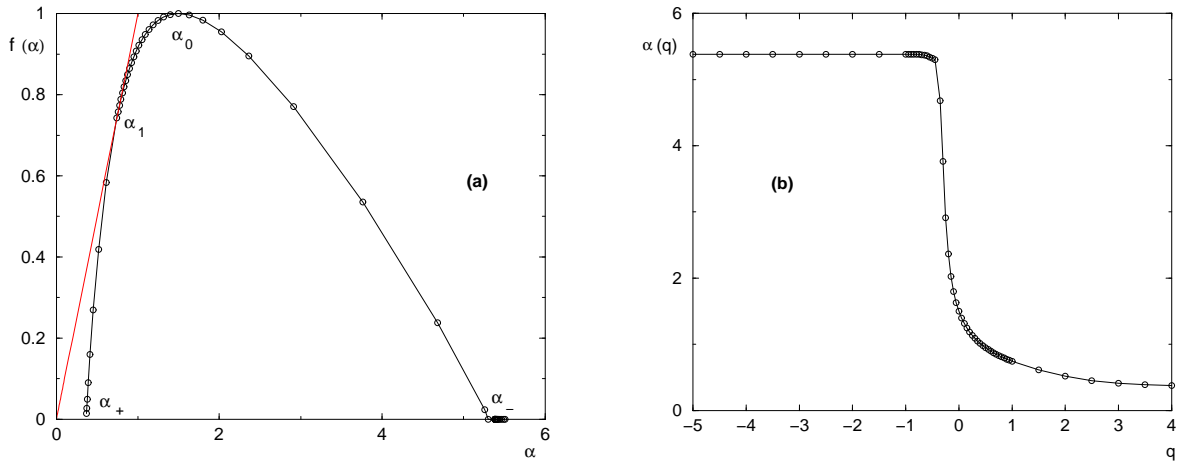


FIG. 7: Cauchy disorder $W = 0.5$ (a) The singularity spectrum $f(\alpha)$ has for termination points $\alpha_+ \simeq 0.37$ and $\alpha_- \simeq 5.3$, for typical value $\alpha_0 \simeq 1.5$ and for tangent point $\alpha_1 = f(\alpha_1) \simeq 0.74$ (b) The corresponding $\alpha(q)$ saturates at a value around $q_+ \simeq 3$.

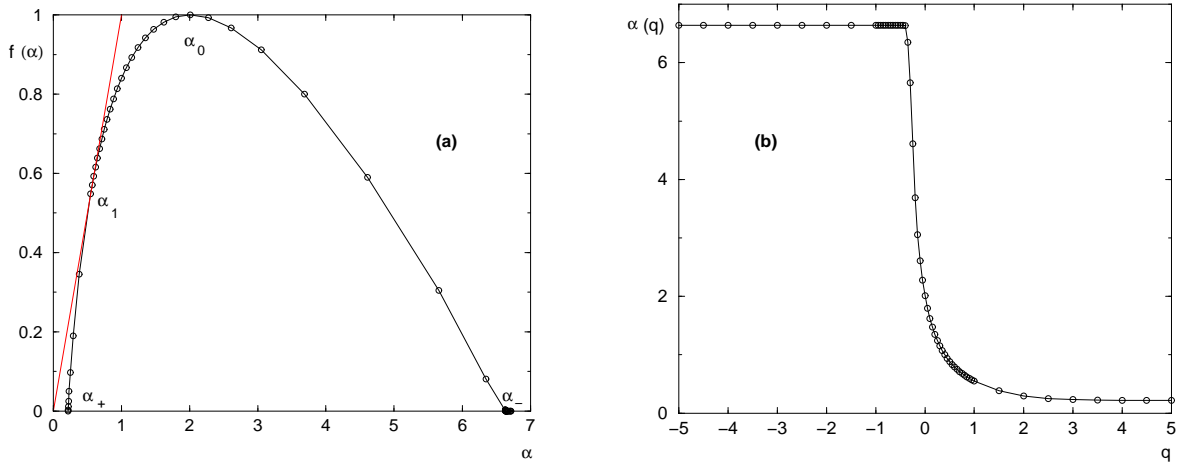


FIG. 8: Cauchy disorder $W = 1$ (a) The singularity spectrum $f(\alpha)$ has for termination points $\alpha_+ \simeq 0.21$ and $\alpha_- \simeq 6.63$, for typical value $\alpha_0 \simeq 2$ and for tangent point $\alpha_1 = f(\alpha_1) \simeq 0.55$ (b) The corresponding $\alpha(q)$ saturates at a value around $q_+ \simeq 2$.

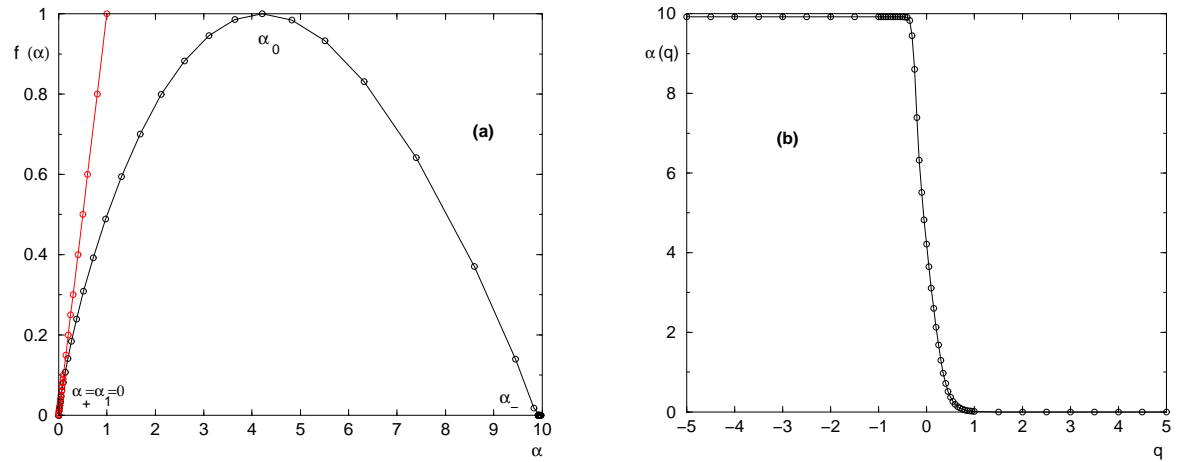


FIG. 9: Cauchy disorder $W = 4$ (a) The singularity spectrum $f(\alpha)$ has for termination points $\alpha_+ \simeq 0$ and $\alpha_- \simeq 9.92$, for typical value $\alpha_0 \simeq 4.21$ and for tangent point $\alpha_1 = f(\alpha_1) \simeq 0$ (b) The corresponding $\alpha(q)$ saturates at the value $q_+ \simeq 1$.

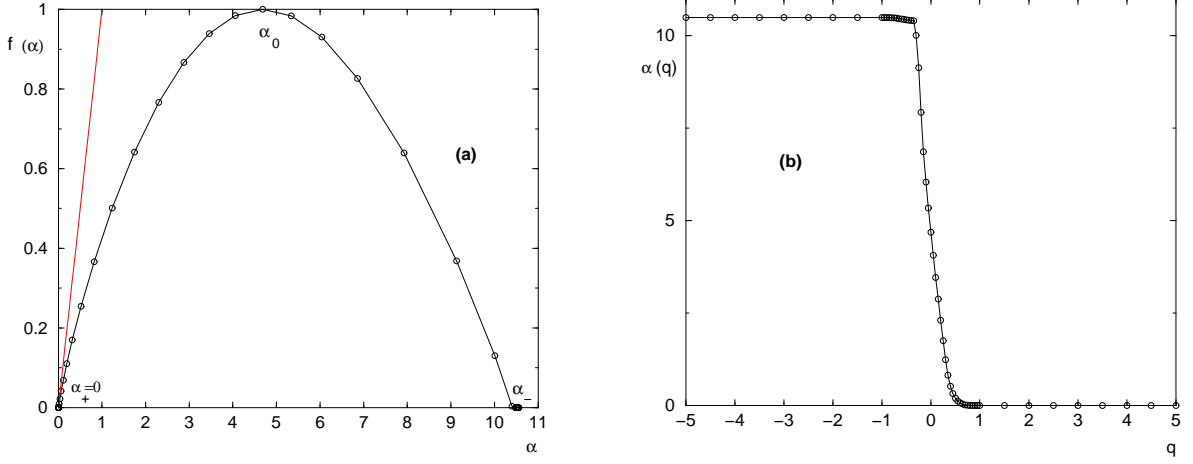


FIG. 10: Cauchy disorder $W = 6$ (a) The singularity spectrum $f(\alpha)$ has for termination points $\alpha_+ = 0$ and $\alpha_- \simeq 10.48$, and for typical value $\alpha_0 \simeq 4.68$ (b) The corresponding $\alpha(q)$ saturates at the value $q_+ \simeq 0.7$.

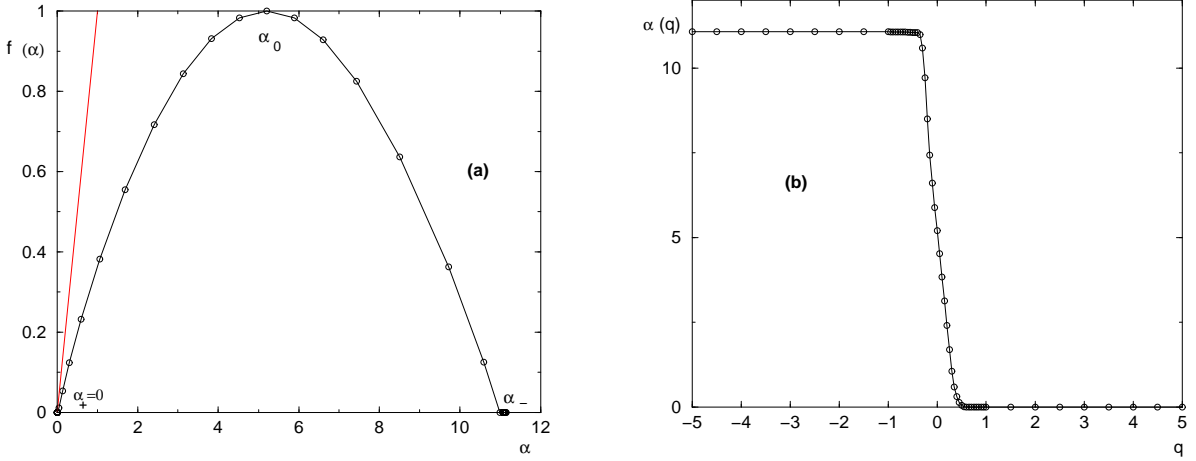


FIG. 11: Cauchy disorder $W = 10$ (a) The singularity spectrum $f(\alpha)$ has for termination points $\alpha_+ = 0$ and $\alpha_- \simeq 11.06$, and for typical value $\alpha_0 \simeq 5.2$ (b) The corresponding $\alpha(q)$ saturates at the value $q_+ \simeq 0.5$.

Appendix A: Reminder on the Directed Polymer on the Cayley tree

1. Reminder on the thermodynamics

The Directed Polymer on a Cayley tree with disorder has been introduced in [38] as a mean-field version of the Directed Polymer in a random medium [39]. The model is defined by the partition function

$$Z_N = \sum_{\mathcal{C}} e^{-\beta E(\mathcal{C})} \quad (\text{A1})$$

where the K^N configurations \mathcal{C} are the paths of N steps on a Cayley tree with coordination number K . The energy $E(\mathcal{C})$ of a path is the sum of the energies of the visited bonds. Each bond has a random energy drawn independently, for instance with the Gaussian distribution

$$\rho(\epsilon) = \frac{1}{\sqrt{2\pi}} e^{-\frac{\epsilon^2}{2}} \quad (\text{A2})$$

This model presents many similarities [38, 40] with the Random Energy Model, introduced by Derrida in the context of spin glasses [41]. It presents a freezing transition at

$$T_c = \frac{1}{\sqrt{2 \ln K}} \quad (\text{A3})$$

The free energy per step $\phi(T)$ coincides with the annealed free energy above T_c and is completely frozen below [38, 40]

$$\phi(T) = \phi_{ann}(T) = -T \ln K - \frac{1}{2T} = -\frac{T}{2T_c^2} - \frac{1}{2T} \quad \text{for } T \geq T_c \quad (\text{A4})$$

$$\phi(T) = -\frac{1}{T_c} \quad \text{for } T \leq T_c \quad (\text{A5})$$

2. Reminder on the finite weights statistics in the frozen phase

The configurations weights in the partition function (Eq. A1) are defined as

$$w_{\mathcal{C}} = \frac{e^{-\beta E_{\mathcal{C}}}}{Z_N(\beta)} \quad (\text{A6})$$

The moments

$$Y_q(N) = \sum_{i=1}^{K^N} w_{\mathcal{C}}^q \quad (\text{A7})$$

have finite disorder-averages in the frozen phase $\mu(T) = T/T_c < 1$ for values $q > \mu(T) = T/T_c$ [42]

$$\overline{Y_q} = \frac{\Gamma(q - \mu(T))}{\Gamma(q)\Gamma(1 - \mu(T))} \quad \text{with } \mu(T) = \frac{T}{T_c} \quad (\text{A8})$$

The density $g(w)$ giving rise to these moments

$$\overline{Y_q} = \int_0^1 dw w^q g(w) \quad (\text{A9})$$

reads [42]

$$g(w) = \frac{w^{-1-\mu}(1-w)^{\mu-1}}{\Gamma(\mu)\Gamma(1-\mu)} \quad (\text{A10})$$

and represents the averaged number of terms of weight w . This density is non-integrable as $w \rightarrow 0$, because in the limit $N \rightarrow \infty$, the number of terms of vanishing weights diverges. The normalization corresponds to

$$\overline{Y_{q=1}} = \int_0^1 dw w g(w) = 1 \quad (\text{A11})$$

3. Reminder on multifractal properties of the weights

In the non-frozen phase, the Y_q of Eq. A7 vanish with the number $M = K^N$ of configurations as power-laws with non-trivial exponents for averaged and typical values, and it is convenient to introduce the multifractal formalism of Eqs 12, 14, 15. In the frozen phase, the finite asymptotic values obtained for $q > \mu(T)$ in Eq. A9 correspond to $\tau_q = 0$, but it is nevertheless interesting to define the multifractal exponents of Eq. 12 for $|q| < \mu$. The fact that the multifractal formalism is appropriate to describe the weights statistics for all values of T , and its exact computation is explained in detail in [45–52]. Here we simply recall the main results, and we refer to [45–52] for more details and discussions. The main point is that the moments Y_q can be rewritten as in terms of the partition functions at inverse temperatures β and $|q|\beta$

$$Y_q(M = K^N) \equiv \frac{\sum_{i=1}^{K^N} e^{-q\beta E_i}}{\left(\sum_{i=1}^{K^N} e^{-\beta E_i}\right)^q} = \frac{Z_N(|q|\beta)}{(Z_N(\beta))^q} = e^{-\beta(|q|F_N(|q|\beta) - qF_N(\beta))} \quad (\text{A12})$$

so that the typical exponents of Eq. 12 are directly given in terms of the free-energy per step of Eq. A5

$$\tau^{typ}(q) = \frac{\beta}{\ln K} [|q| \phi(|q|\beta) - q \phi(\beta)] \quad (\text{A13})$$

In the following, we thus quote the final results for the typical singularity spectrum $f(\alpha)$ in the various phases, and we present the numerical results obtained on trees of sizes $10 \leq N \leq 22$ to show that such sizes are sufficient to obtain reliable results by comparison with the exact forms (more details on the numerical procedure can be found in Appendix B).

a. Non-Frozen Phase $\mu \equiv \frac{T}{T_c} > 1$

In the non-frozen phase, the left and right termination points read

$$\begin{aligned} \alpha_+ &= \left(1 - \frac{1}{\mu}\right)^2 \\ \alpha_- &= \left(1 + \frac{1}{\mu}\right)^2 \end{aligned} \quad (\text{A14})$$

and the typical singularity spectrum is exactly Gaussian on the interval $\alpha_+ < \alpha < \alpha_-$ where it exists

$$f_{T>T_c}^{typ}(\alpha) = \frac{\mu^2}{4} (\alpha - \alpha_+) (\alpha_- - \alpha) \quad (\text{A15})$$

The terminating values α_{\pm} are associated with the values $q_{\pm} = \pm\mu$. In the interval $q_- = -\mu \leq q \leq q_+ = +\mu$, the value $\alpha(q)$ dominating the saddle point calculation of Eq. 15 is simply linear in q

$$\alpha(q_- = -\mu \leq q \leq q_+ = +\mu) = \left(1 + \frac{1}{\mu^2}\right) - \frac{2q}{\mu^2} \quad (\text{A16})$$

The typical value corresponding to $q = 0$ in Eq. A16

$$\alpha_0 = \left(1 + \frac{1}{\mu^2}\right) \quad (\text{A17})$$

is the point where the singularity spectrum reaches its maximum $f(\alpha_0) = 1$ (Eq. 19). Finally the value $q = 1$ where the singularity spectrum is tangent to the line $\alpha = f(\alpha)$ (Eq. 20) correspond to (Eq. A16)

$$\alpha_1 = 1 - \frac{1}{\mu^2} = f(\alpha_1) \quad (\text{A18})$$

The numerical results shown on Fig. 12 are in agreement with these expressions for $\mu = 2$.

b. Critical point $\mu \equiv \frac{T}{T_c} = 1$

In the limit $\mu \equiv \frac{T}{T_c} \rightarrow 1^+$, the above singularity spectrum has the following properties : the left terminating point α_+ of Eq. A14 vanishes

$$\alpha_+ = 0 \quad (\text{A19})$$

together with the tangent point to the line $\alpha = f(\alpha)$ (Eq. A18)

$$\alpha_1 = f(\alpha_1) = 0 \quad (\text{A20})$$

The corresponding numerical results for $\mu = 1$ are shown on Fig. 13.

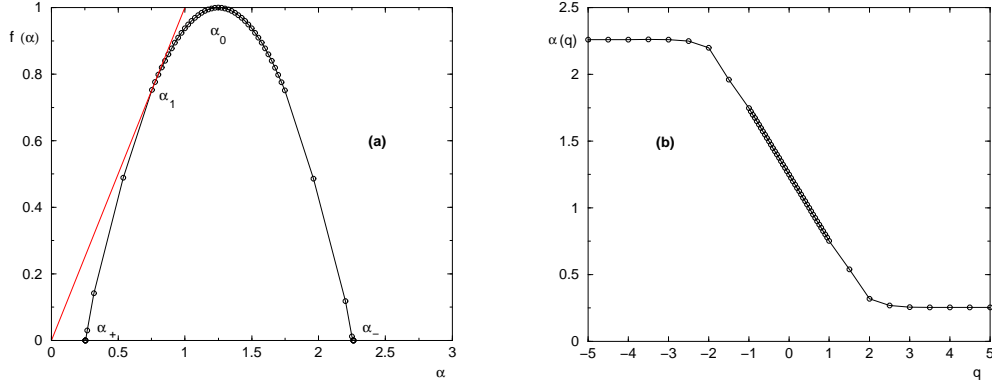


FIG. 12: Directed Polymer in the non-frozen phase at $\mu \equiv T/T_c = 2$ (see section A 3 a) : (a) Singularity spectrum $f(\alpha)$: the terminating points are $\alpha_+ = 0.25$ and $\alpha_- = 2.25$, the typical value is $\alpha_0 = 1.25$, the line $\alpha = f(\alpha)$ is tangent at $f(\alpha_1) = \alpha_1 = 0.75$. (b) The saddle-point $\alpha(q)$ remains frozen at α_+ for $q > q_+ = 2$ and to α_- for $q < q_- = -2$.

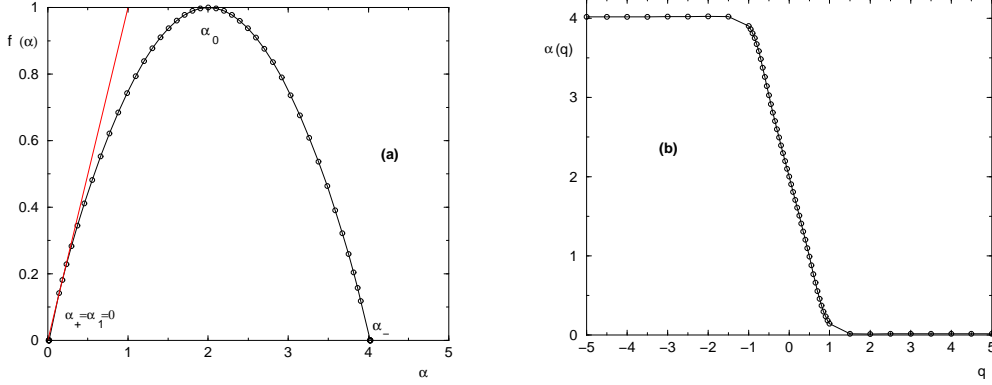


FIG. 13: Directed Polymer at the critical point for $\mu \equiv T/T_c = 1$ (see section A 3 b) : (a) Singularity spectrum $f(\alpha)$: the terminating points are $\alpha_+ = 0$ and $\alpha_- = 4$, the typical value is $\alpha_0 = 2$, the line $\alpha = f(\alpha)$ is tangent at the origin $f(\alpha_1) = \alpha_1 = 0$. (b) The saddle-point $\alpha(q)$ remains frozen at α_+ for $q > q_+ = 1$ and to α_- for $q < q_- = -1$.

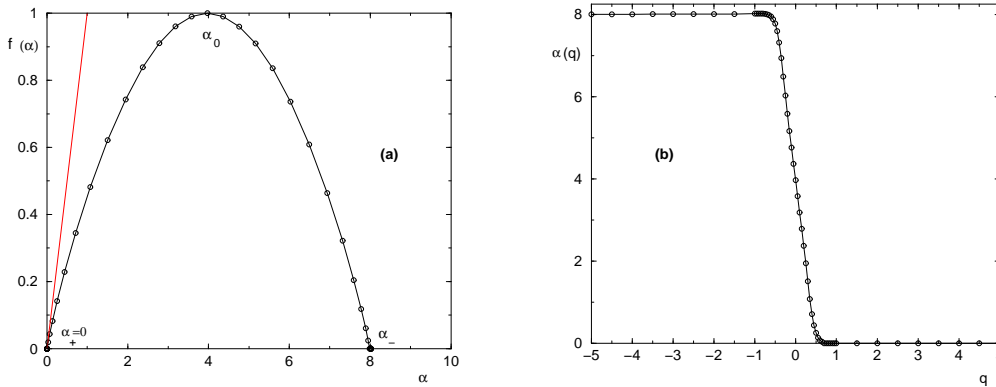


FIG. 14: Directed Polymer in the frozen phase at $\mu \equiv T/T_c = 0.5$ (see section A 3 c) : (a) Singularity spectrum $f(\alpha)$: the terminating points are $\alpha_+ = 0$ and $\alpha_- = 8$, the typical value is $\alpha_0 = 4$. (b) The saddle-point $\alpha(q)$ remains frozen at α_+ for $q > q_+ = 0.5$ and to α_- for $q < q_- = -0.5$.

c. *Frozen Phase* $\mu \equiv \frac{T}{T_c} < 1$

In the frozen phase, the left termination point is zero

$$\alpha_+ = 0 \quad (\text{A21})$$

and the right termination point is

$$\alpha_- = \frac{4}{\mu} \quad (\text{A22})$$

On the interval $\alpha_+ = 0 < \alpha < \alpha_-$ where it exists, the typical singularity spectrum is again exactly Gaussian

$$f_{T < T_c}^{typ}(\alpha) = \frac{\mu^2}{4} \alpha (\alpha_- - \alpha) \quad (\text{A23})$$

The left terminating value $\alpha_+ = 0$ is reached for $q_+ = \mu$ and the right terminating value α_- is reached for $q_- = -\mu$. In the interval $q_- = -\mu \leq q \leq q_+ = +\mu$, the value $\alpha(q)$ dominating the saddle point calculation of Eq. 15 is again linear in q

$$\alpha(q_- = -\mu \leq q \leq q_+ = +\mu) = \frac{2}{\mu} - \frac{2q}{\mu^2} \quad (\text{A24})$$

The typical value corresponding to $q = 0$ in Eq. A24 is

$$\alpha_0 = \frac{2}{\mu} \quad (\text{A25})$$

Note that here the value $q = 1$ is already in the frozen region $1 > q_+ = \mu$, so that the singularity spectrum is completely below the line $\alpha = f(\alpha)$. The numerical results shown on Fig. 14 are in agreement with these expressions for $\mu = 0.5$.

Appendix B: Details concerning the numerical evaluation of $f(\alpha)$

In each sample with N generations, we compute the $M = K^N$ weights of Eq. 10, from which we obtain immediately the parameters I_q of Eq. 11. The corresponding typical exponents $\tau^{typ}(q)$ of Eq. 12 are then obtained by the following three parameters fit of the average over disordered samples

$$\overline{\ln I_q(M)} \simeq -\tau_q^{typ} \ln M + c_0 \ln(\ln M) + c'_0 \quad (\text{B1})$$

i.e. τ_q^{typ} is obtained as the coefficient of the leading linear term. The presence of the subleading term (c_0) is important only in the regions where τ_q nearly vanishes $\tau_q \sim 0$, whereas in the regions where τ_q is not small, a direct linear fit could be acceptable and would give nearly the same numerical value for τ_q .

The typical multifractal spectrum $f^{typ}(\alpha)$ could in principle be obtained from $\tau^{typ}(q)$ by some numerical procedure to perform the Legendre transform of Eq. 15, but this method has a lot of numerical drawbacks [44]. We have thus followed the standard method of Ref [44], with the simplification that we consider only boxes of size $L = 1$ in the notation of Ref [44], i.e. we do not use any coarse-graining with various box sizes, but we analyse instead the scaling with respect to the total number of boxes $M = K^N$ from our data obtained of various sizes N . The main idea of Ref [44] is to construct the following normalized q -measures from the initial measure defined by the weights of Eq. 10

$$w_j^{(q)} \equiv \frac{[w_j]^q}{\sum_{j'} [w_{j'}]^q} \quad (\text{B2})$$

Of course $q = 1$ correspond to the initial measure $w_j^{(q=1)} = w_j$. The denominator corresponds to I_q of Eq. 11. It is then useful to introduce

$$\begin{aligned} F_q(M) &= - \sum_{j=1}^M w_j^{(q)} \ln w_j^{(q)} \\ A_q(M) &= - \sum_{j=1}^M w_j^{(q)} \ln w_j \end{aligned} \quad (\text{B3})$$

$F_q(M)$ represents the Shannon entropy of the q -measure, whereas $A_q(M)$ represents the averaged log of the initial weight $\ln w_j$ with respect to the q -measure. From Eq. B2, one obtains immediately the simple relation

$$F_q(M) = qA_q(M) + \ln I_q(M) \quad (\text{B4})$$

which, after the division by the scaling factor $(\ln M)$, exactly corresponds to the Legendre transform relation of Eq. 15. Numerically, one only has to compute I_q and A_q , whereas F_q can be immediately obtained from them by Eq. B3. The averages over the disordered samples of the two observables of Eq. B3 can be analyzed by the following three parameters fits

$$\begin{aligned} \overline{F_q(M)} &\simeq f_q \ln M + c_1 \ln(\ln M) + c'_1 \\ \overline{A_q(M)} &\simeq \alpha_q \ln M + c_2 \ln(\ln M) + c'_2 \end{aligned} \quad (\text{B5})$$

The leading coefficients (α_q, f_q) then constitutes a parametric representation of the typical singularity spectrum $f(\alpha)$ as q varies. The presence of the subleading terms (c_1, c_2) are important only in the regions where f_q nearly vanishes $f_q \sim 0$, whereas in the regions where f_q is not small, direct linear fits could be acceptable and would give nearly the same numerical values for (α_q, f_q) .

All the singularity spectra $f(\alpha)$ shown on the figures correspond to the parametric representation (α_q, f_q) obtained by the procedure just described. We have also presented our corresponding data for α_q to show the freezing phenomena in the parameter q . In Appendix A, we find that the singularity spectra obtained via this numerical analysis are in agreement with the available exact results.

-
- [1] P.W. Anderson, Phys. Rev. 109, 1492 (1958).
 - [2] D.J. Thouless, Phys. Rep. 13, 93 (1974) ; D.J. Thouless, in "Ill Condensed Matter" (Les Houches 1978), Eds R. Balian *et al.* North-Holland, Amsterdam (1979).
 - [3] B. Souillard, in "Chance and Matter" (Les Houches 1986), Eds J. Souletie *et al.* North-Holland, Amsterdam (1987).
 - [4] I.M. Lifshitz, S.A. Gredeskul and L.A. Pastur, "Introduction to the theory of disordered systems" (Wiley, NY, 1988).
 - [5] B. Kramer and A. MacKinnon, Rep. Prog. Phys. 56, 1469 (1993).
 - [6] P. Markos, Acta Physica Slovaca 56, 561 (2006).
 - [7] F. Evers and A.D. Mirlin, Rev. Mod. Phys. 80, 1355 (2008).
 - [8] E. Abrahams, P.W. Anderson, D.C. Licciardello and T.V. Ramakrishnan, Phys. Rev. Lett. 42, 673 (1979).
 - [9] R. Abou-Chacra, P.W. Anderson and D.J. Thouless, J. Phys. C : Solid State Physics 6, 1734 (1973) (see also R. Abou-Chacra and D. J. Thouless, J. Phys. C: Solid State Phys. 7, 65 (1974)).
 - [10] H. Kunz and B. Souillard, J. Physique Lettres 44, L411 (1983).
 - [11] A.D. Mirlin and Y.V. Fyodorov, Nucl. Phys. B 366, 507 (1991).
 - [12] B. Derrida and G.J. Rodgers, J. Phys. A : Math. Gen. 26, L457 (1993).
 - [13] J.D. Miller and B. Derrida, J. Stat. Phys. 75, 357 (1994).
 - [14] C. Monthus and T. Garel, J. Phys. A 42, 075002 (2009).
 - [15] B. Shapiro, Phys. Rev. Lett. 50, 747 (1983).
 - [16] J.T. Chalker and S. Siak, J. Phys. : Condens. Matt. 2, 2671 (1990)
 - [17] P.M. Bell and A. MacKinnon, J. Phys. : Condens. Matt. 6, 5423 (1994).
 - [18] G. Biroli, G. Semerjian and M. Tarzia, Prog. Theor. Phys. Suppl. 184, 187 (2010).
 - [19] D.M. Basko, I.L. Aleiner, B.L. Altshuler, Annals of Physics 321, 1126 (2006) and Phys. Rev. B 76, 052203 (2007).
 - [20] B.L. Altshuler, Y. Gefen, A. Kamenev and L.S. Levitov, Phys. Rev. Lett. 78, 2803 (1997).
 - [21] P.G. Silvestrov Phys. Rev. Lett. 79, 3994 (1997).
 - [22] P.G. Silvestrov Phys. Rev. E 58, 5629 (1998).
 - [23] P.G. Silvestrov, Phys. Rev. B 64, 113309 (2001).
 - [24] I.V. Gornyi, A.D. Mirlin and D.G. Polyakov, Phys. Rev. Lett. 95, 206603 (2005).
 - [25] V. Oganesyan and D.A. Huse, Phys. Rev. B 75, 155111 (2007).
 - [26] C. Monthus and T. Garel, Phys. Rev. B 81, 134202 (2010).
 - [27] M. Znidaric, T. Prosen, and P. Prelovsek, Phys. Rev. B 77, 064426 (2008).
 - [28] A. Karahalios, A. Metavitsiadis, X. Zotos, A. Gorczyca, and P. Prelovsek, Phys. Rev. B 79, 024425 (2009); O.S. Barisic and P. Prelovsek, Phys. Rev. B 82, 161106 (R) (2010).
 - [29] T. C. Berkelbach and D. R. Reichman, Phys. Rev. B 81, 224429 (2010)
 - [30] A. Pal and D. A. Huse, Phys. Rev. B 82, 174411 (2010)
 - [31] O.S. Barisic and P. Prelovsek, Phys. Rev. B 82, 161106 (2010).
 - [32] R. Landauer, Philos. Mag. 21, 863 (1970).
 - [33] P. W. Anderson, D. J. Thouless, E. Abrahams and D. S. Fisher Phys. Rev. B 22, 3519 (1980).
 - [34] P. W. Anderson and P.A. Lee, Suppl. Prog. Theor. Phys. 69, 212 (1980).

- [35] J.M. Luck, “Systèmes désordonnés unidimensionnels” , Alea Saclay (1992).
- [36] A.D. Stone and A. Szafer, IBM J. Res. Dev. 32, 384 (1988).
- [37] M. Aizenman and S. Warzel, arXiv:1010.2673.
- [38] B. Derrida and H. Spohn, J. Stat. Phys., **51**, 817 (1988).
- [39] T. Halpin-Healy and Y.-C. Zhang, Phys. Rep. 254, 215 (1995).
- [40] J. Cook and B. Derrida, J. Stat. Phys. **63**, 505 (1991).
- [41] B. Derrida, Phys. Rev. B 24, 2613 (1981).
- [42] B. Derrida, “Non-self-averaging effects in sums of random variables, spin glasses, random maps and random walks”, in “On three levels” Eds M. Fannes et al (1994) New-York Plenum Press.
- [43] C. Monthus and T. Garel, Phys. Rev. E 75, 051119 (2007).
- [44] A. Chhabra and R.V. Jensen, Phys. Rev. Lett. 62, 1327 (1989).
- [45] C. Chamon, C. Mudry, and X.-G. Wen, Phys. Rev. Lett. 77, 4194 (1996)
- [46] H. E. Castillo, C. Chamon, E. Fradkin, P. M. Goldbart and C. Mudry, Phys. Rev. B 56, 10668 (1997)
- [47] D. Carpentier and P. Le Doussal, Phys. Rev. Lett. 81, 2558 (1998) and Nucl. Phys. B 588, 565 (2000).
- [48] D. Carpentier and P. Le Doussal, Phys. Rev. E 63, 026110 (2001).
- [49] Y.V. Fyodorov and J.P. Bouchaud, JETP Letters 86, 487 (2007); J. Phys. A: Math. Theor. 41 324009 (2008) and J.Phys. A Math Theor. 41, 371001 (2008).
- [50] Y. V. Fyodorov, JSTAT P07022 (2009).
- [51] Y. V Fyodorov, P. Le Doussal and A. Rosso, JSTAT P10005 (2009).
- [52] Y. V. Fyodorov, Physica A 389, 4229 (2010).
- [53] P. Lloyd, J. Phys. C 2, 1717 (1969).